Contents lists available at ScienceDirect

International Journal of Electronics and Communications

Regular paper

An innovative fractal monopole MIMO antenna for modern 5G applications

Sabah Hassan Ghadeer [a], Sharul Kamal Abd.Rahim [a], Mohammad Alibakhshikenari [b,*],
Bal S. Virdee [c], Taha A. Elwi [d,*], Amjad Iqbal [e,f], Muath Al-Hasan [f]

[a] Faculty of Engineering, School of Electrical Engineering, Universiti Teknologi Malaysia (UTM), Malaysia
[b] Department of Signal Theory and Communications, Universidad Carlos III de Madrid, 28911 Leganés, Madrid, Spain
[c] Center for Communications Technology, London Metropolitan University, London N7 8DB, UK
[d] International Applied and Theoretical Research Center (IATRC), Baghdad Quarter, Iraq
[e] Institut National de la Recherche Scientifique (INRS), Montréal, QC H5A1K6, Canada
[f] Department of Network and Communications Engineering, Al Ain University, Al Ain 64141, United Arab Emirates

ARTICLE INFO

ABSTRACT

Proposed in this paper is the design of an innovative and compact antenna array which based on four radiating elements for multi-input multi-output (MIMO) antenna applications used in 5G communication systems. The radiating elements are fractal curves excited using an open-circuited feedline through a coplanar waveguide (CPW). The feedline is electromagnetically coupled to the inside edge of the radiating element. The array's impedance bandwidth is enhanced by inserting a ground structure composed of low–high-low impedance between the radiating elements. The low-impedance section of the ground is a staircase structure that is inclined at an angle to follow the input feedline. This inter-radiating element essentially suppresses near-field radiation between adjacent radiators. A band reject filter based on a composite right/left hand (CRLH) structure is mounted at the back side of the antenna array to reduce mutual coupling between the antenna elements by choking surface wave propagations that can otherwise degrade the radiation performance of the array antenna. The CRLH structure is based on the Hilbert fractal geometry, and it was designed to act like a stop band filter over the desired frequency bands. The proposed antenna array was fabricated and tested. It covers the frequency bands in the range from 2 to 3 GHz, 3.4–3.9 GHz, and 4.4–5.2 GHz. The array has a maximum gain of 6. 2dBi at 3.8 GHz and coupling isolation better than −20 dB. The envelope correlation coefficient of the antenna array is within the acceptable limit. There is good agreement between the simulated and measured results.

1. Introduction

The use of antenna arrays at sub-6 GHz frequency bands are now needed to implement multi-input multi-output (MIMO) systems required for 5G wireless communication systems [1]. MIMO is a highly effective technique for increasing the channel capacity. The challenge remains in developing compact antenna arrays necessary to reduce the form factor MIMO systems. A smaller form factor is needed to realize inconspicuous 5G base-stations [2] and to use 5G systems inside public spaces like arenas and sports ground as well as to improve inbuilding wireless mobile coverage and enhance streaming speeds [3,4]. By reducing the spacing of the antennas in an array result in stronger mutual coupling between the radiating elements that adversely affects

the orthogonality between different data streams and deteriorates the systems channel capacity [5,6].Therefore, to ensure the high performance of MIMO systems is a significant challenge.

Numerous decoupling methods have been proposed to reduce mutual coupling. This includes space diversity [7], neutralization-line [8], parasitic resonance decoupling [9], self-isolation [10], polarization diversity [11], and high-order mode decoupling [12]. Although in these MIMO antennas high isolation is achievable, however they require a large space. To save the system space, antennas using a shared radiator have attracted much interest [13–20]. Designs with multiport antenna pairs have been reported and investigated using polarization orthogonality methods [12–15], self-decoupling [16], and lumped elements [17]. A self-decoupled antenna pair has been reported recently in [18] to
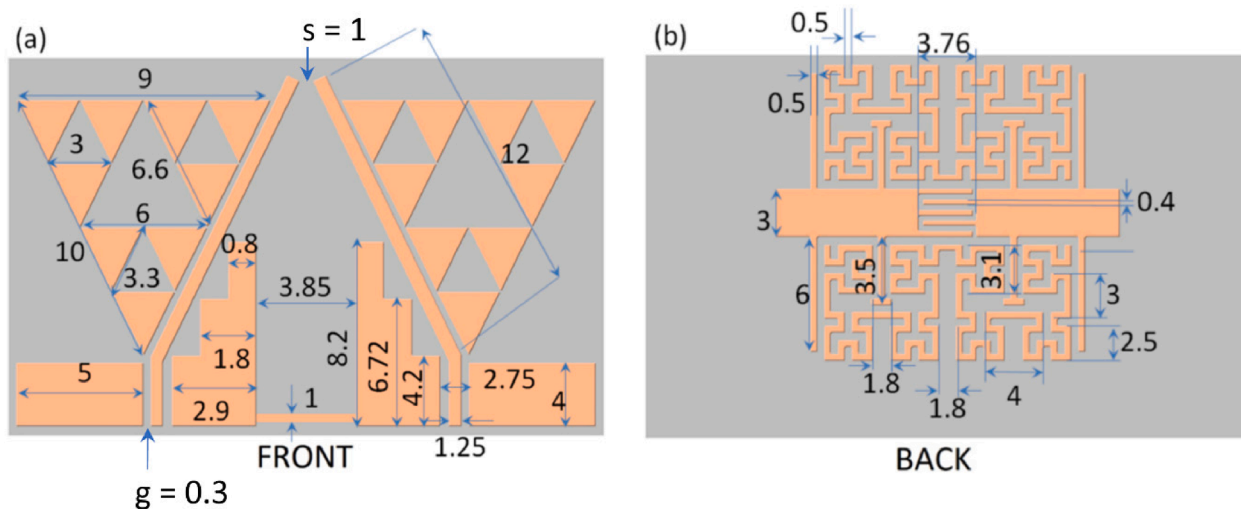

Fig. 1. Geometry of the proposed two-element MIMO antenna array (units in millimeter), (a) Front view, and (b) Back view.

Fig. 2. Sierpiński fractals of order 0 to 2.

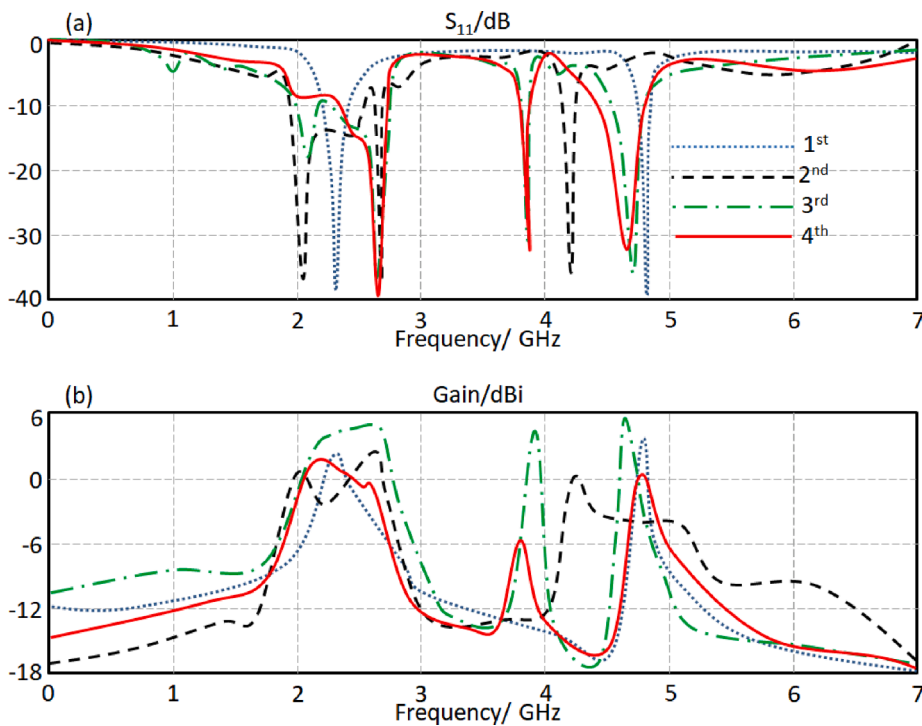**Fig. 3.** Performance of Sierpiński fractal antenna of order 1 to 4: (a) reflection coefficient (S_{11}), and (b) antenna gain.
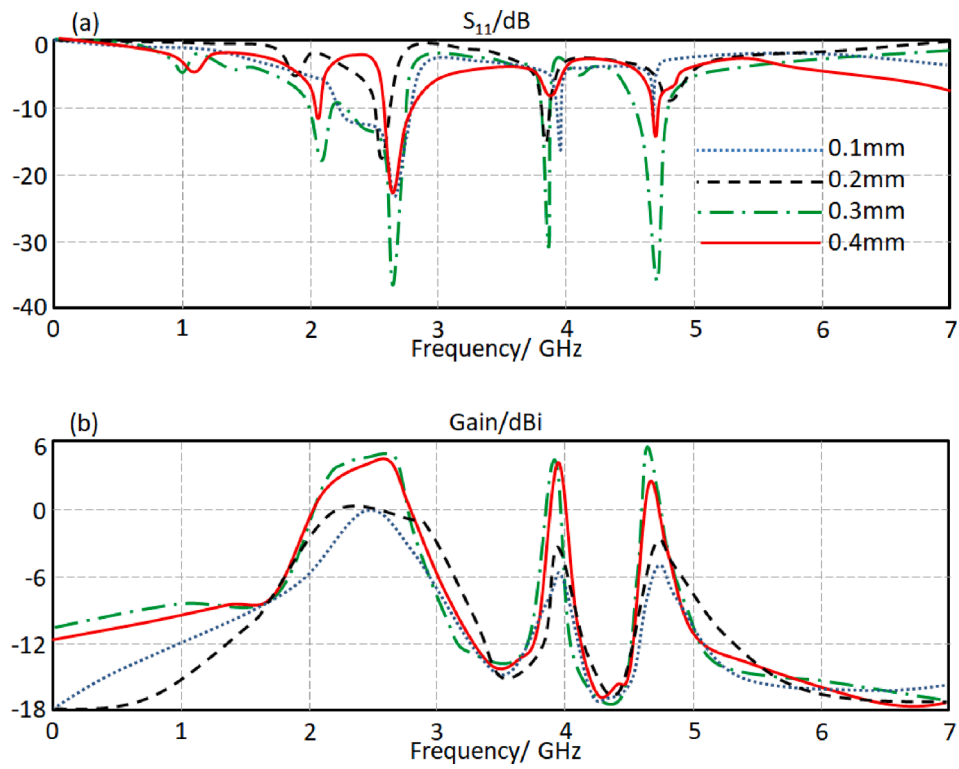
Fig. 4. Antenna array's performance with different coupling gap (g) size: (a) reflection coefficient (S_{11}), and (b) antenna gain.
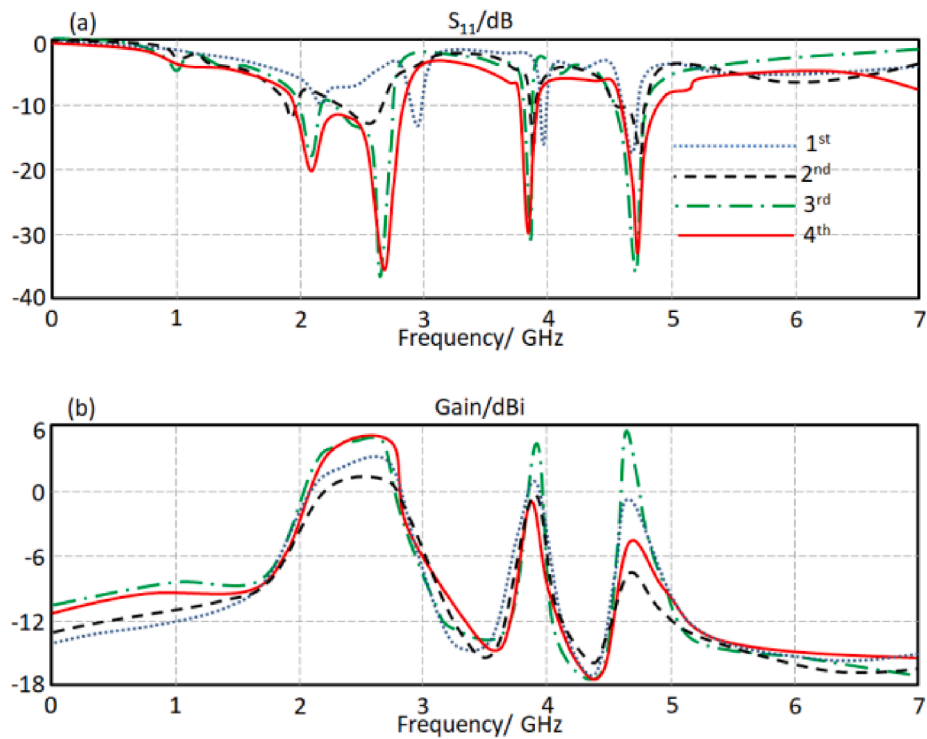

Fig. 5. Antenna array's performance as a function of staircase step number: (a) reflection coefficient (S_{11}), and (b) antenna gain.
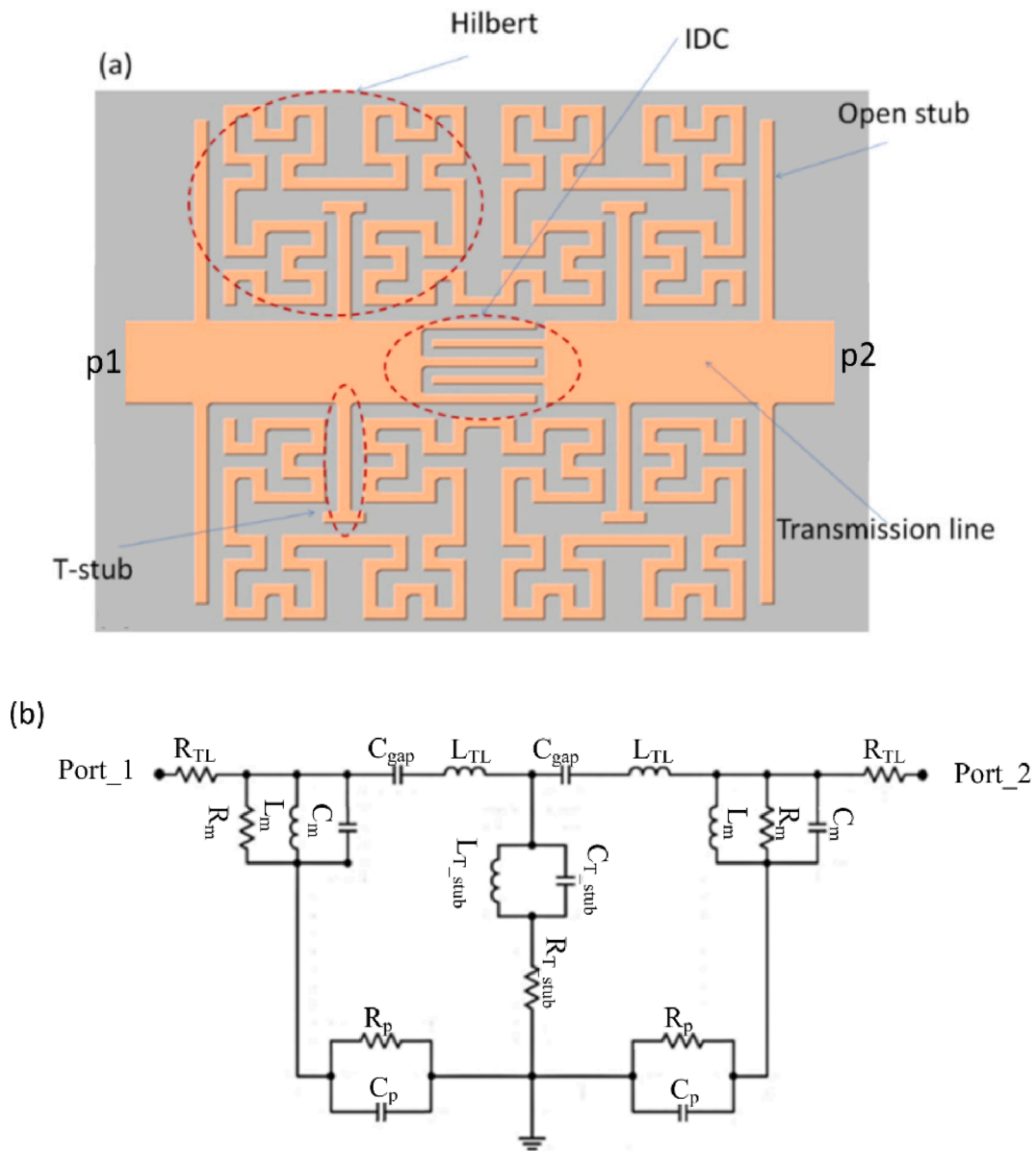
Fig. 6. CRLH filter structure: (a) numerical model, and (b) equivalent circuit model.

achieve an inter-antenna isolation of better than 11.5 dB with shared radiator based common mode and the differential mode. Common and differential mode technique has been also used to reduce the mutual coupling in [19] by incorporating an inductive strip into two closely placed patch antennas. This method is a good solution to decouple antennas in MIMO systems. Mutual coupling in [20] was reduced by inserting an electromagnetic bandgap (EBG) structure between the antenna elements. With this technique the EBG structures must be inserted away from the antenna's edge to achieve an acceptable reflection coefficient. Inter-element spacing with this technique is made greater than $0.5\lambda_o$. This results in a larger array size and limits the scan angle for beam steering arrays. It has been shown in [21] the use of metamaterial (MTMs) structures in antenna arrays can help to enhance the reduction of mutual coupling effects. Examination of prior work shows the design of a MIMO antenna with concurrent characteristics of broadband, high isolation, and compact size is still a challenge.

In this work, a design of a 2D antenna array is proposed for sub-6 GHz MIMO wireless systems. Individual monopole patch antennas in the array are based on a Sierpiński fractal geometry [22]. The purpose of using fractal curves was to achieve an array that exhibits gain-bandwidth enhancement. Incorporated in the array is filtering functionality that is contributed by a 2D composite right/left hand (CRLH) structure which is located immediately underneath the antenna array. The CRLH structure is based on Hilbert fractal geometry and designed to mitigate surface wave propagation to reduce mutual coupling between the antenna elements in the array. The antenna array prototype design radiates energy over the frequency bands of $2-3$ GHz, $3.4-3.9$ GHz, and $4.4-5.2$ GHz. The antenna array has an average gain of 5.5 dBi in the specified frequency bands. Size of the overall antenna array $40 \times 30 \times 1.67$ mm^3 suitable for mobile wireless devices.

This work is organized as followings: Discussed in section 2 is the geometry of the proposed antenna array including the CRLH filtering structure and presented are the array's simulation performance in terms of reflection coefficient, antenna gain and inter-radiating element insolation. In section 3 discussed is the array's radiation patterns, correlation and diversity properties. Antenna array of matrix size 4×4 design is discussed in section 4. In section 5 the measured results of the fabricated 4×4 antenna array are given. The paper is concluded in section 6.
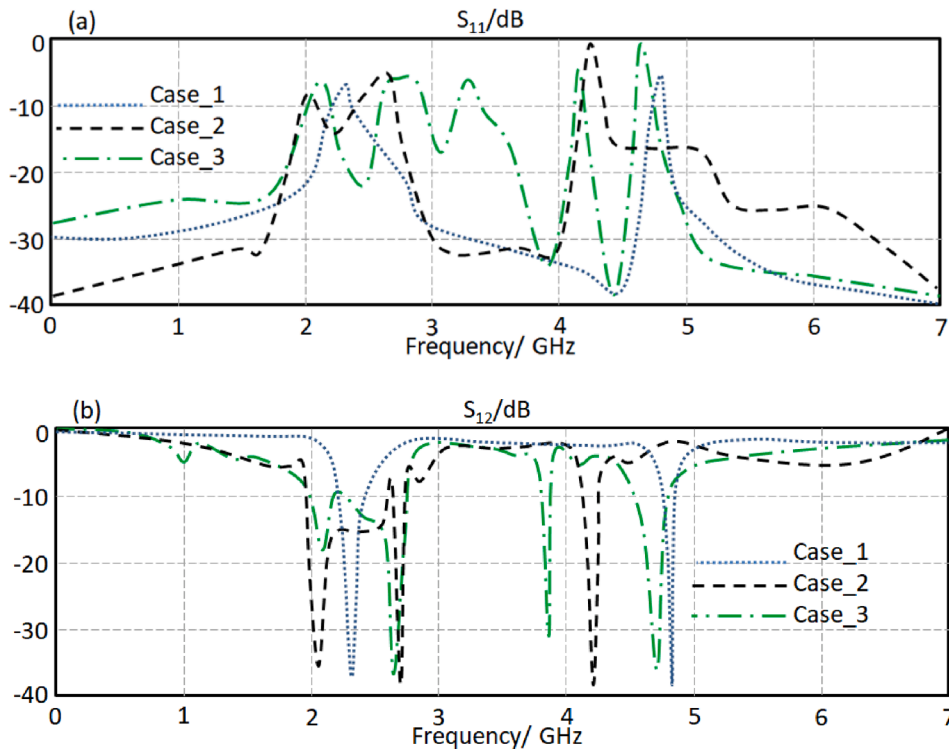
Fig. 7. The S-parameter response under Case-1 to Case-3 on the CRLH structure's performace: (a) reflection coefficient (S_{11}), and (b) transmission coefficient (S_{12}).

Table 1
Lumped values of the equivalent circuit of the CRLH filter.

Lumped element	value	Lumped element	value
$L_{T.L}$	0.1 nH	L_{T_stub}	0.09 nH
$R_{T.L}$	50 Ω	C_m	1.9 pF
C_{T_stub}	40 pF	C_{gap}	2.2 pF
$L/2$	1.1 nH	R_p	22 Ω
C	35 pF	C_p	3.1 pF
R_m	70 Ω	L_m	0.2 nH

2. Structure of antenna array

Geometry of the proposed antenna array of matrix size 2×2 is shown in Fig. 1. The radiation patch element is represented by a repeating pattern of inverted triangles that repeat at a different scale. The repeating pattern is also known as Sierpiński triangle fractal where the number of k triangles remaining after the n-th iteration in the process of recursively removing triangles is given by

$$k = 3^{n-1} \tag{1}$$

Let N_n be the number of black triangles after iteration n, L_n the length of a side of a triangle, and A_n the fractional area which is black after the n-th iteration. Then

$$N_n = 3^n \tag{2a}$$

$$L_n = \left(\frac{1}{2}\right)^n = 2^{-n} \tag{2b}$$

In relation to the original triangle, after the n-th iteration, the area of the Sierpiński triangle is given by

$$A_n = L_n^2 N_n = \left(\frac{3}{4}\right)^n \tag{3}$$

The reason for using the fractal-based patch antenna was to increase the impedance bandwidth of the array. The fractal antenna is

electromagnetically excited through an open-circuited microstrip line through a coplanar waveguide. The coplanar waveguide was used to reduce dispersion effects and for broadband performance. The feedline of characteristic 50 Ω impedance is electromagnetically coupled to the inside edge of the radiating element. The technique used here to enhance the array's impedance bandwidth is achieved by coupling the adjacent radiating elements through a transmission line structure which is composed of low–high-low impedance. The low-impedance section is electromagnetically coupled to one side of the input feedline and has a three-step staircase shape. The length of the interconnect is such that there is phase coherency at the two radiating elements. On the backside of the antenna array immediately below it is located a structure that exhibits composite right/left hand characteristics. The structure consists of inter-digitally coupled microstrip lines with high impedance open-circuited stubs located at both ends, as shown in Fig. 1(b). Located approximately mid-way are short T-shaped open-circuited lines that are electromagnetically coupled to Hilbert fractal shaped curves. The function of the CRLH structure is to mitigated surface wave propagation and thus reduce unwanted mutual coupling between the two radiating elements. Unwanted coupling can undermine the radiation performance of the array which can adversely impact on the wireless systems channel capacity. The proposal two-element antenna array is fabricated on an FR4 substrate with a dielectric constant is 4.3, thickness of 1.67 mm and loss-tangent of 0.025. The overall size of the antenna array is $40 \times 30 \times 1.67$ mm^3. Dimensions of the antenna structure are annotated in Fig. 1.

2.1. Simulation results

The Sierpiński triangle is created through an iterative algorithm defined by Eqn.(1)-(3). Starting with an equilateral inverted triangle, the midpoints of each side are found and connected to form a smaller triangle which is then removed. The same process is then applied to the remaining triangles at each stage. The reflection coefficient and gain performance of Sierpiński fractal of iteration order 1 to 4 were studied using CST Microwave Studio. Sierpiński fractal of iteration order

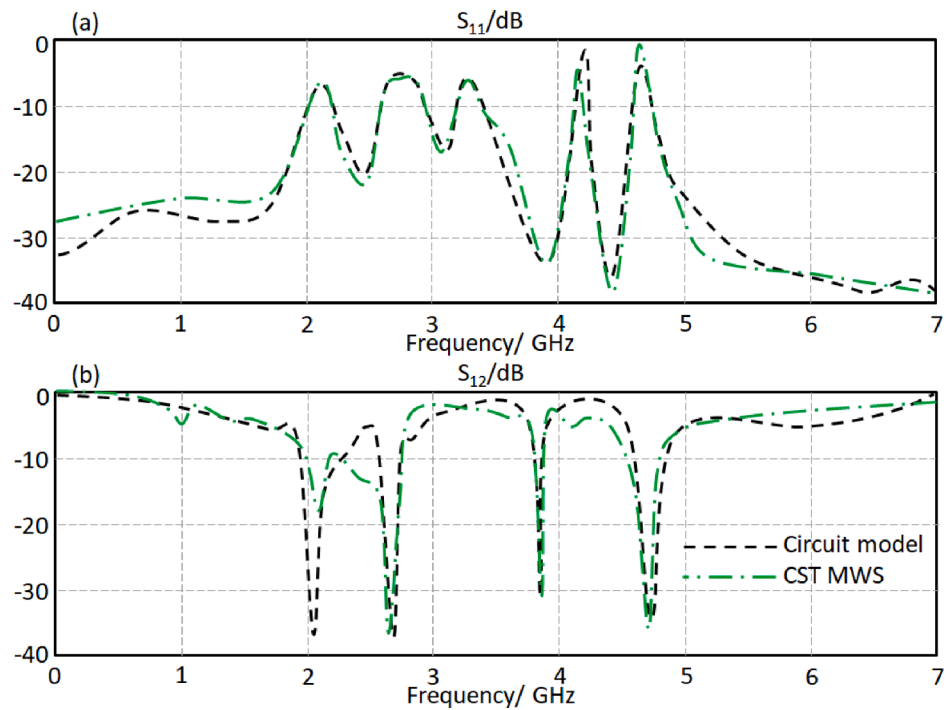**Fig. 8.** Comparison between the simulated (using CST Microwave Studio) and equivalent circuit model of the filter structure on the array's performace: (a) reflection coefficient (S_{11}), and (b) transmission coefficient (S_{12}).

Fig. 9. Effect of the gap (s) between the two-element antenna array's performace: (a) reflection coefficient (S_{11}), and (b) transmission coefficient (S_{12}).

Fig. 10. Effect of the CRLH band stop structure on the antenna array's performance: (a) reflection coefficient (S_{11}), and (b) transmission coefficient (S_{12}).

Fig. 11. Effect of CPW ground connection on the antenna array's performance: (a) reflection coefficient (S_{11}), and (b) transmission coefficient (S_{12}).

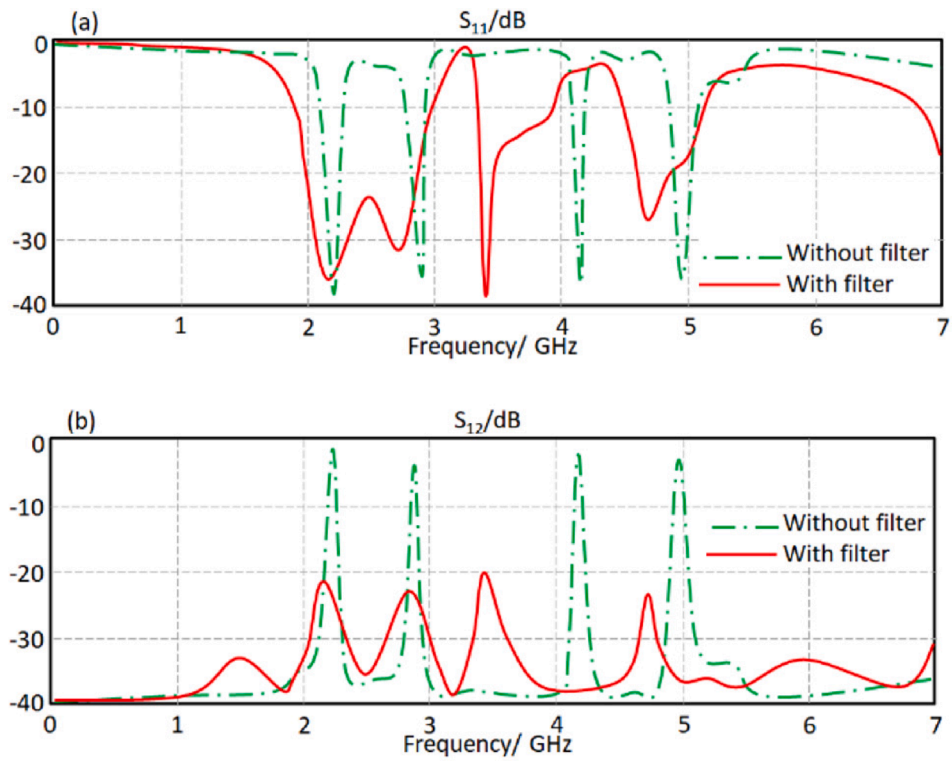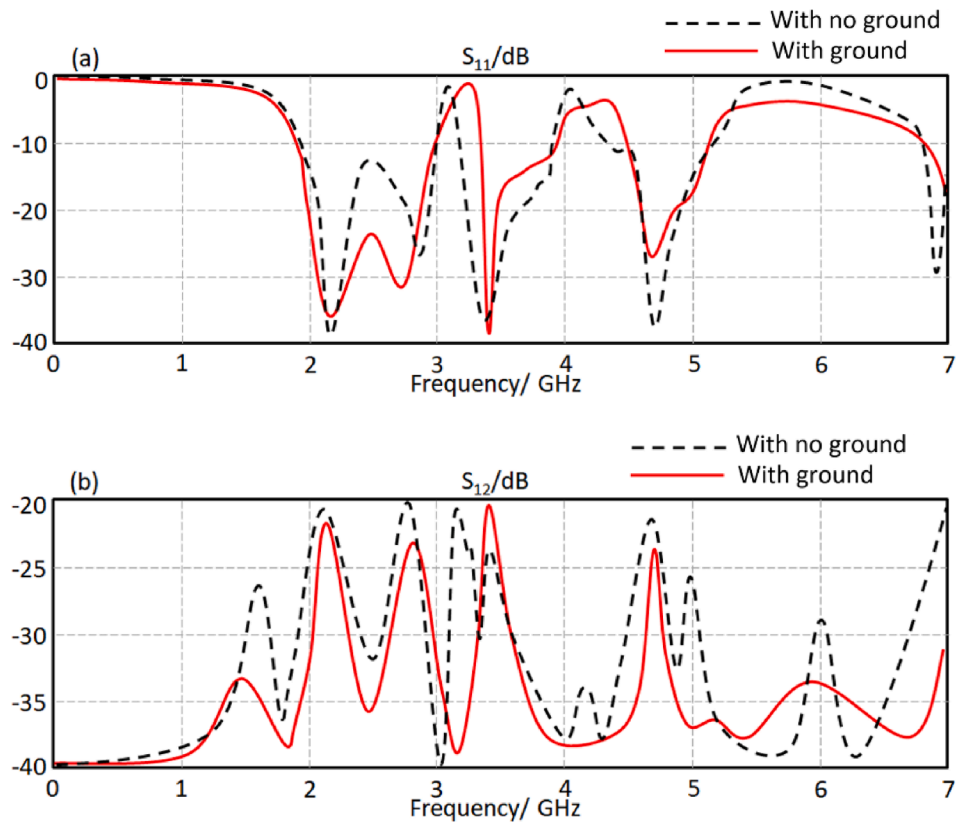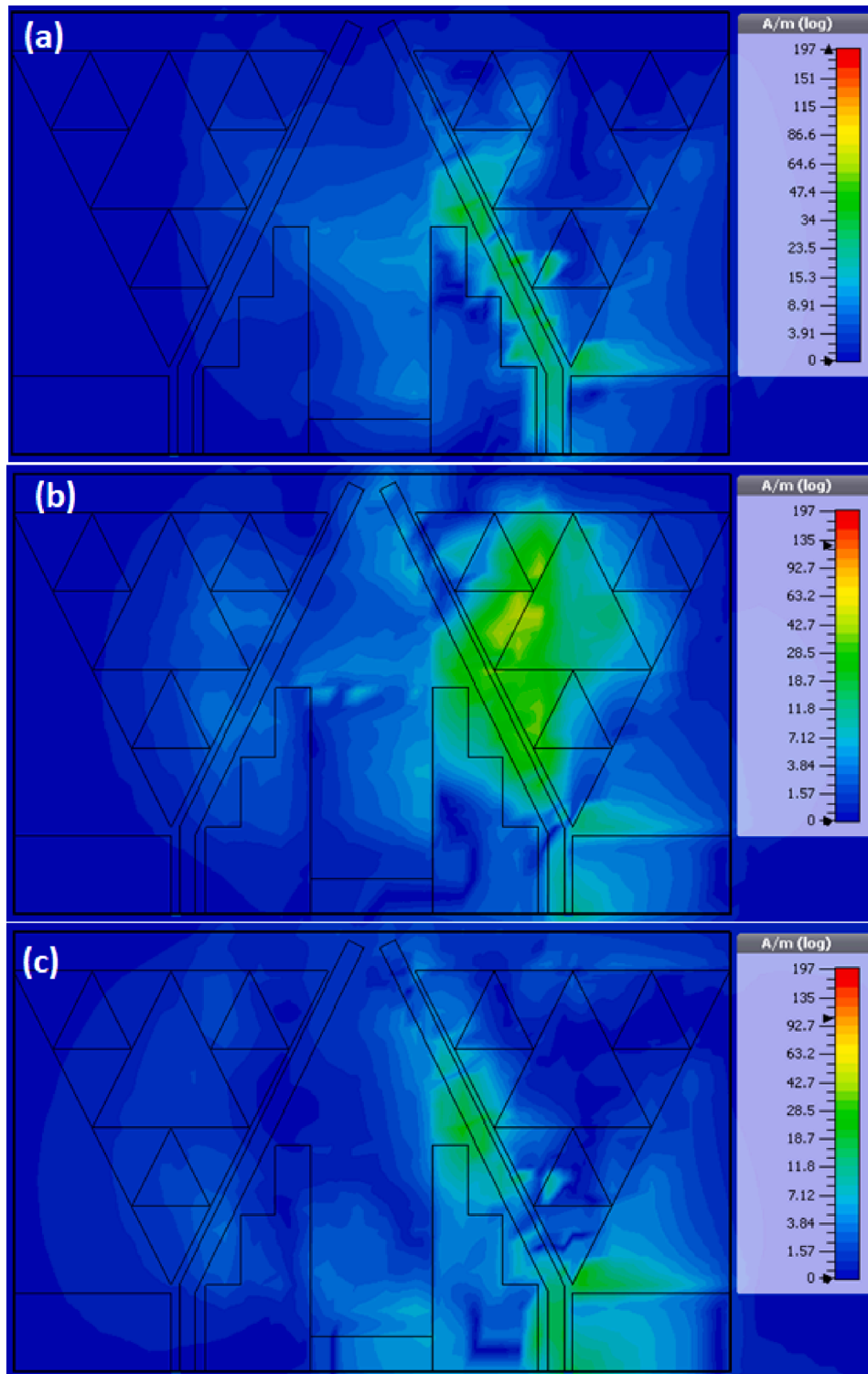**Fig. 12.** Surface current distributions over the two-element array: (a) 2.5 GHz, (b) 3.85 GHz, and (c) 4.5 GHz.

0 antenna is a regular patch antenna resembling an inverted triangle. In iteration order 1 fractal the single inverted triangle of order 0 is replaced by three inverted triangles occupying the same area as order 0. In iteration order 2, each of the three triangles of order 1 are replaced by three smaller triangles, etc. as shown in Fig. 2. The simulated results in Fig. 3 shows the antenna is a triband resonator. Fig. 3(a) shows the increase in fractal order improves the impedance bandwidth of the first and last band. However, Fig. 3(b) shows the increase in fractal order can undermine the antenna's gain. The gain is optimum for fractal of order 3,

which provides a peak gain of 5.5 dBi at the three bands. In the proposed antenna design fractal of order 3 was chosen.

The parametric study of the coupling gap (g) between the fractal antenna and the microstrip feedline was carried out to gain more insight of its affect. The coupling gap was varied from 0.1 mm to 0.4 mm and the corresponding change in the reflection coefficient response and gain are shown in Fig. 4. From Fig. 4(a) it is evident that the coupling gap of 0.3 mm significantly improves the impedance matching. However, further increase in the coupling gap degrades the reflection coefficient.
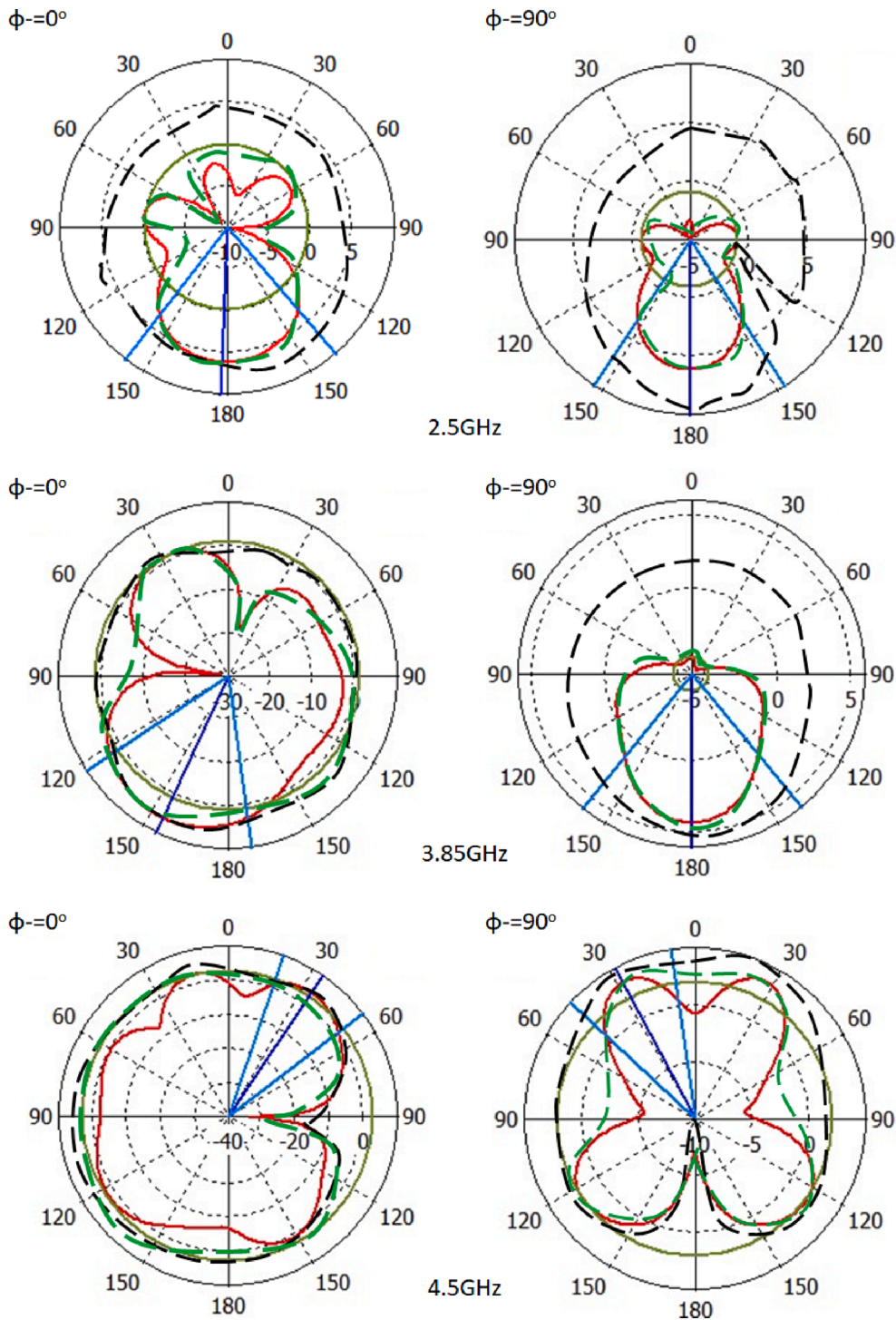
Fig. 13. Simulated far-field radiation patterns at 2.5 GHz, 3.85 GHz, and 4.5 GHz. Note: Black long dash is for the antenna array with no filter and no CPW ground, the red sold line is for the antenna array with filter and no CPW ground, green dotted line is for CPW grounded antenna array with no filter, and the black dotted line is for CPW grounded antenna array with filter.

Fig. 4(b) shows optimum gain is achieved with coupling gap size of 0.3 mm at the three bands of the antenna. Therefore, a coupling gap size of 0.3 mm was used in the design of the proposed antenna.

The effect the inclusion of the staircase structure that interconnects the two coplanar waveguide feedlines was investigated. Fig. 5 shows how the reflection coefficient and gain response of the 2×2 antenna array is affected when the number of steps of the staircase is increased from 1 to 4. It is evident from Fig. 5(a) the response shown the optimum number of steps is 3 as any more steps deteriorate the reflection

coefficient response. The impedance bandwidth of the 3 and 4 steps are roughly comparable. Fig. 5(b) shows at the lower band a 4-step structure provides comparable gain as a 3-step structure however a higher gain is achieved in the middle and upper bands of the array with a 3-step staircase structure.

2.2. Filter design

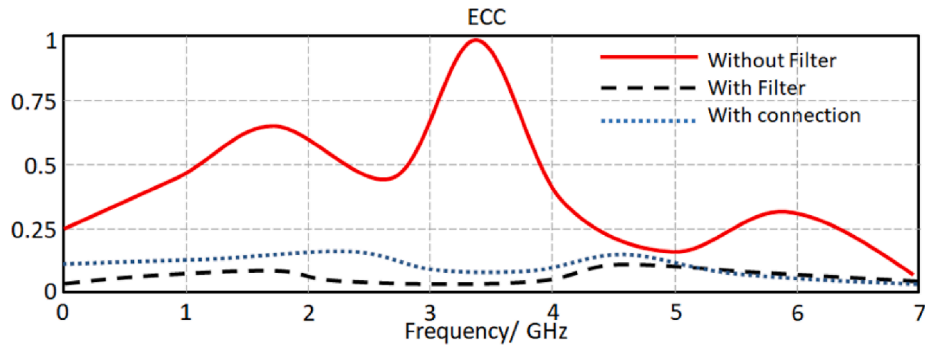The proposed antenna array was backed with a planar structure that

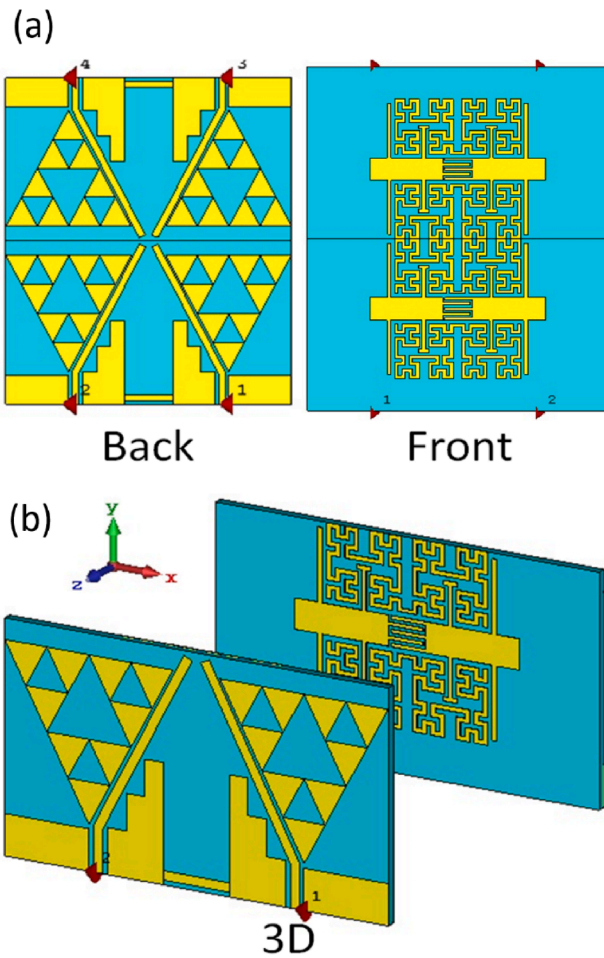**Fig. 14.** Antenna array's envelope correction coefficient (ECC).

Fig. 15. Four-element antenna array based on the proposed antenna: (a) front and back view, and (b) isometric view of the front and backside of the array.

had band stop characteristics over the array's operational frequency band. The proposed filtering structure shown in Fig. 6(a) is a composite right/left hand (CRLH) structure whose function is to mitigate unwanted mutual coupling between the antenna elements by choking surface wave propagation. Unwanted coupling can degrade the radiation performance of the array antenna. The filtering structure comprises inter-digitally coupled microstrip lines. Located at both ends of the coupled lines are high impedance open-circuited stubs, as shown in Fig. 6(a). Short T-shaped open-circuited lines are placed approximately mid-way of the coupled lines that are electromagnetically coupled to Hilbert fractal shaped curves. The equivalent circuit model of the CRLH filter is shown in Fig. 6(b).

The three sections of the filtering structure are, namely Case-1 the open-circuited stub, Case-2 the interdigital capacitor, and Case-3 the Hilbert curve coupled to the open-circuited T-shaped stub. Fig. 7 shows the reflection coefficient (S_{11}) and transmission coefficient (S_{12}) response of the three sections constituting the proposed filter. The transmission coefficient indicates the isolation between the two ports (p1 & p2) indicated in Fig. 6. Fig. 7(a) shows the reflection coefficient for Case-1 is better than −20 dB except between 2.1 and 2.7 GHz and 4.7–4.85 GHz. With reference to Case-2, the reflection coefficient is better than −20 dB except between 1.8 and 2.8 GHz and 4.2–5.3 GHz. For Case-3, the reflection coefficient is better than −20 dB except between 1.75 and 3.7 GHz, 4.15–4.3 and 4.6–4.85 GHz. Fig. 7(b) shows for Case-1 the isolation is greater than 10 dB between 2.3 and 2.45 GHz and 4.7–4.8 GHz. The isolation for Case-2 is greater than 10 dB between 1.95 and 2.7 GHz and 4.2–4.3 GHz. For Case-3, the isolation is greater than 10 dB between 2 and 2.75 GHz, 3.7–3.8 GHz and 4.6–4.8 GHz.

The values of the equivalent circuit model in Fig. 6(b) was determined by parameter extraction method as decribed in [23] using by genetic algorithm. Table 1 shows the parameter values obtained of the equivalent circuit model. Fig. 8 compares the simulated reflection coefficient and transmission coefficient response of the filter with the circuit model. It can be observed there is excellent agreement between the two responses.

3. Two-Port MIMO array system design

A parametric study was carried out to determine how the antenna array's performance including radiation pattern is affected by the gap between the antennas, inclusion of CRLH filtering structure, and coplanar waveguide ground.

3.1. Effect of antenna gap

The effect of the gap (s), shown in Fig. 1(a), between the two antenna's was studied to determine the impact of the coupling and the fringing fields on the overall antenna array's performance. In this study CRLH filter was not applied on the backside of the array. The results of varying the gap (s) in step size of 5 mm from 1 mm to 16 mm is shown in Fig. 9. The results of the study shows the gap (s) has a significant effect on the reflection coefficient and transmission coefficient in terms of magnitide and resonance freuency. Fig. 9(a) shows the reflection coefficient worsens with increasing gap above 11 mm. The reflection coefficient are similar with a gap size of 1 mm and 6 mm. This outcome is reflected in the isolation results in Fig. 9(b). The isolation is optimum with a gap size of 1 mm which is equivalent to 0.15λ at free-space frequency of 2 GHz.

3.2. Effect of the CRLH filter

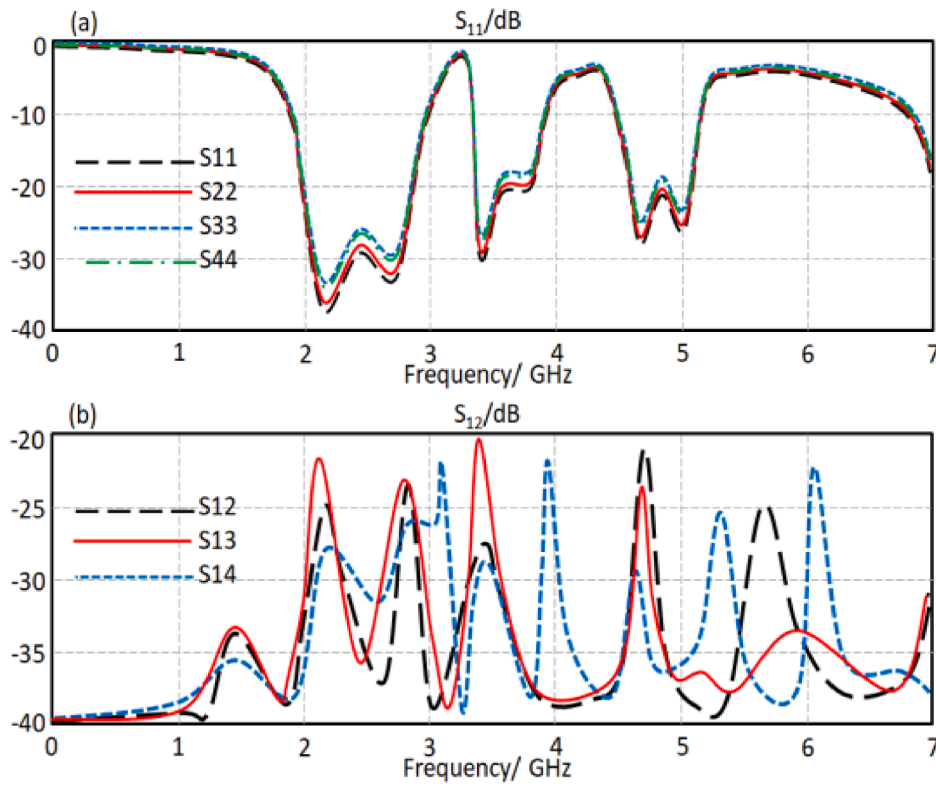Mutual coupling in antenna arrays is attributed to near-field effects

Fig. 16. S-parameters of the proposed 4 × 4 antenna array: (a) reflection coefficient (S_{11}), and (b) transmission coefficient (S_{12}).
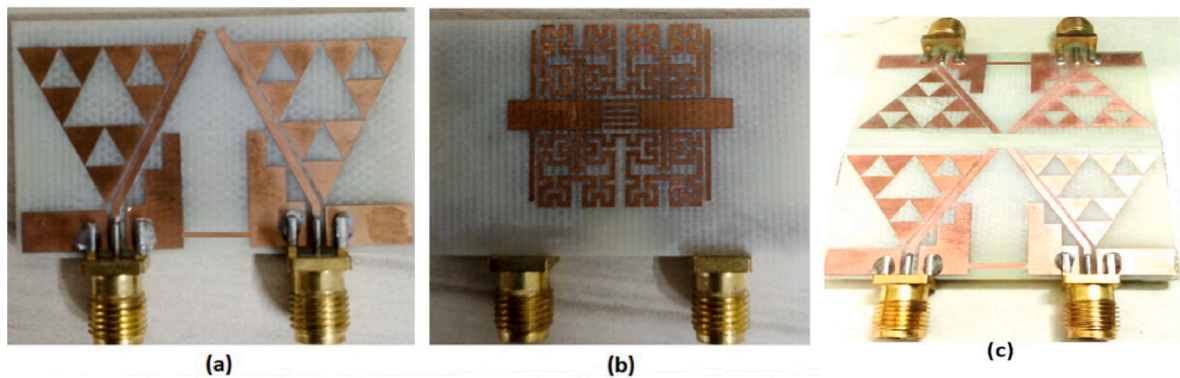

Fig. 17. Fabricated prototype of the proposed antenna array: (a) front view of 2 × 2 array, (b) back view 2 × 2 array, (c) isometric view of 4 × 4 array.

and surface waves which can adversely affect the far-field radiation characteristics of the antenna array. Unwanted mutual coupling is severe when the antennas in the array are closely spaced to reduce the form factor of the array. Under these conditions it becomes imperative to suppress the unwanted mutual coupling. The approach taken here to do this was to apply a CRLH band stop structure at the backside of the two-element antenna array. The results without and with the CRLH filtering structure is shown in Fig. 10. With no CRLH structure the reflection coefficient exhibits four narrow resonance responses and the isolation between the two antennas is minimal. However, with the CRLH structure a broader impedance bandwidth is realized and the isolation between the radiators is significantly improved by approximately 20 dB.

3.3. Effect of coplanar waveguide ground

The effect of grounding the coplanar waveguide was investigated. Fig. 11 shows how the reflection coefficient and isolation are affected with and without the CPW ground. With the ground connection the

reflection coefficient of the first band is improved however the impedance bandwidth of the middle band reduced. Although the impedance bandwidth of the third band is maintained however the impedance match across this band is reduced but it's acceptable (<-10 dB). With the ground connection the isolation is moderately reduced across each band. Grounding is important to stop the buildup charge that can build up to dangerous levels and result in electrostatic discharge. The surface current distribution in Fig. 12 shows a better understanding of the isolation mechanism. The current distribution is shown at 2.5 GHz, 3.85 GHz, and 4.5 GHz when one of the ports is excited. It is evident that staircase ground essentially blocks energy interacting with the adjacent radiating element.

3.4. Effect CPW and CRLH on antenna radiation patterns

The antenna array's simulated radiation patterns in the E-plane (ϕ = 0°) and H-plane (ϕ = 90°) with and without filter structure, and with and without CPW ground connection at 2.5 GHz, 3.5 GHz and
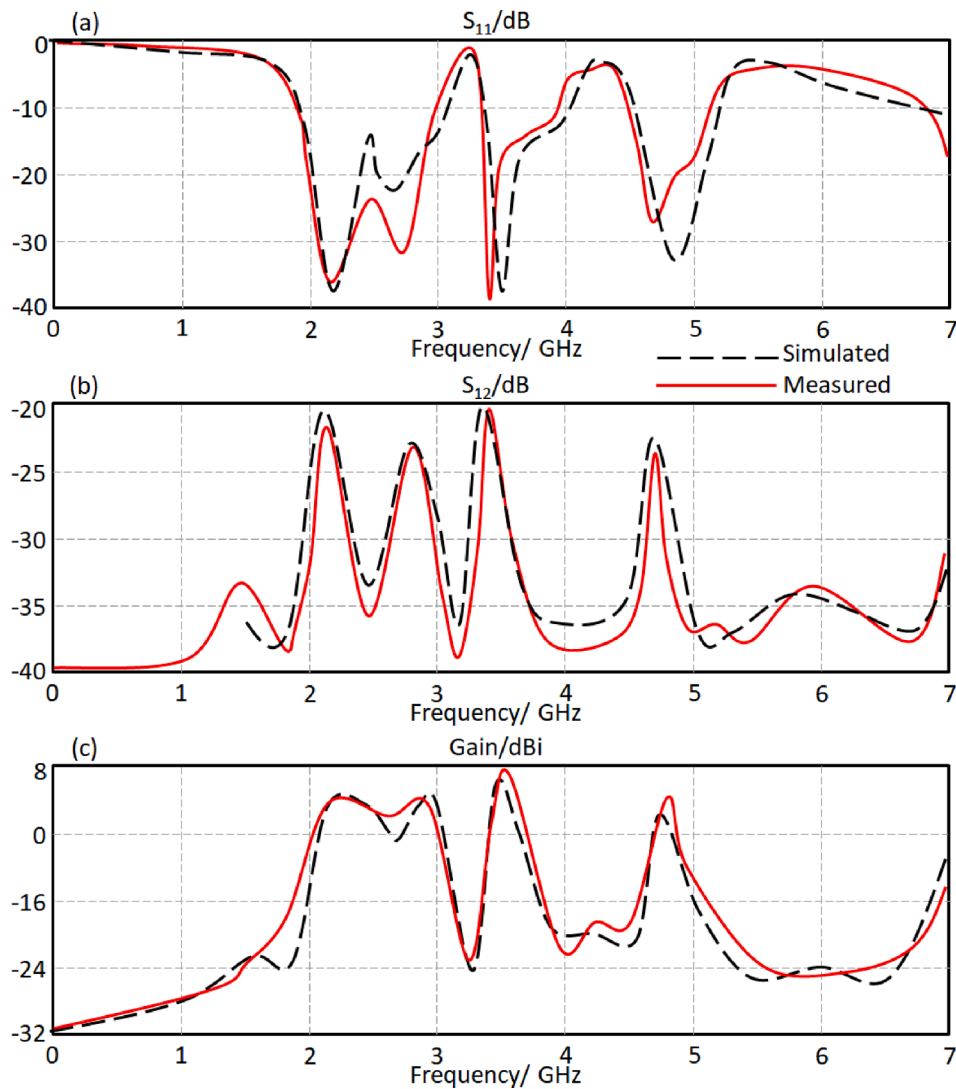
Fig. 18. Measured results of the four-element antenna array: (a) reflection coefficient (S_{11}), (b) transmission coefficient (S_{12}), and (c) antenna gain.

4.5 GHz are shown in Fig. 13. At 2.5 GHz the antenna radiates energy directionally. At 3.85 GHz and 4.5 GHz in the E-plane the antenna predominately omnidirectionally. In the H-plane at 3.85 GHz the antenna radiates directionally. However, at the three spot frequencies when the CPW is grounded and with the CRLH filter it radiates omnidirectionally.

3.5. Correlation and diversity properties

To fully characterize antenna arrays the parameters namely envelope correlation coefficient (ECC) and mean effective gain (MEG) needs to be evaluated. ECC is determined using Eq. (4) [24].

$$\rho_e = \frac{\left| \iint_{4\pi} \left[\overrightarrow{F}_1(\theta,\varphi)^* \overrightarrow{F}_2(\theta,\varphi) \right] d\Omega \right|^2}{\iint_{4\pi} \left| \overrightarrow{F}_1(\theta,\varphi) \right|^2 d\Omega \iint_{4\pi} \left| \overrightarrow{F}_2(\theta,\varphi) \right|^2 d\Omega} \tag{4}$$

where $\overrightarrow{F}_1(\theta,\varphi)$ and $\overrightarrow{F}_2(\theta,\varphi)$ is the three-dimensional far-field radiation of the two antennas. There are two techniques to calculate ECC, i.e., from the 3-D radiation pattern or from S-parameters. The ECC here was calculated from the 3-D radiation pattern. The mean effective gain

(MEG) of the antenna array was calculated using Eq. (5) [4]

$$MEG = \int_0^{2\pi}$$
$$\times \int_0^{\pi} \left(\frac{XPR}{1+XPR} G_\theta(\theta,\varphi) P_\theta(\theta,\varphi) + \frac{1}{1+XPR} G_\varphi(\theta,\varphi) P_\varphi(\theta,\varphi) \right) \sin\theta d\theta d\varphi \tag{5}$$

where XPR is the cross-polarization power ratio, the theta and phi components of the incoming signal powers are represented by as P_θ and P_φ, respectively. The antenna gains in the theta and phi directions are described by G_θ and G_φ. Fig. 14 shows ECC under three conditions, namely the antenna array without CRLH filter, with CRLH filter and with CPW ground connection. It is evident that without the magnitude of ECC is poor between 1 GHz and 4 GHz. The mean effective gain for the array with CRLH filter and grounded CPW was approximately 0 dBi.

4. Four-Element antenna array

A four-element antenna array was designed based on the proposed two-element array described in the above sections. The front and
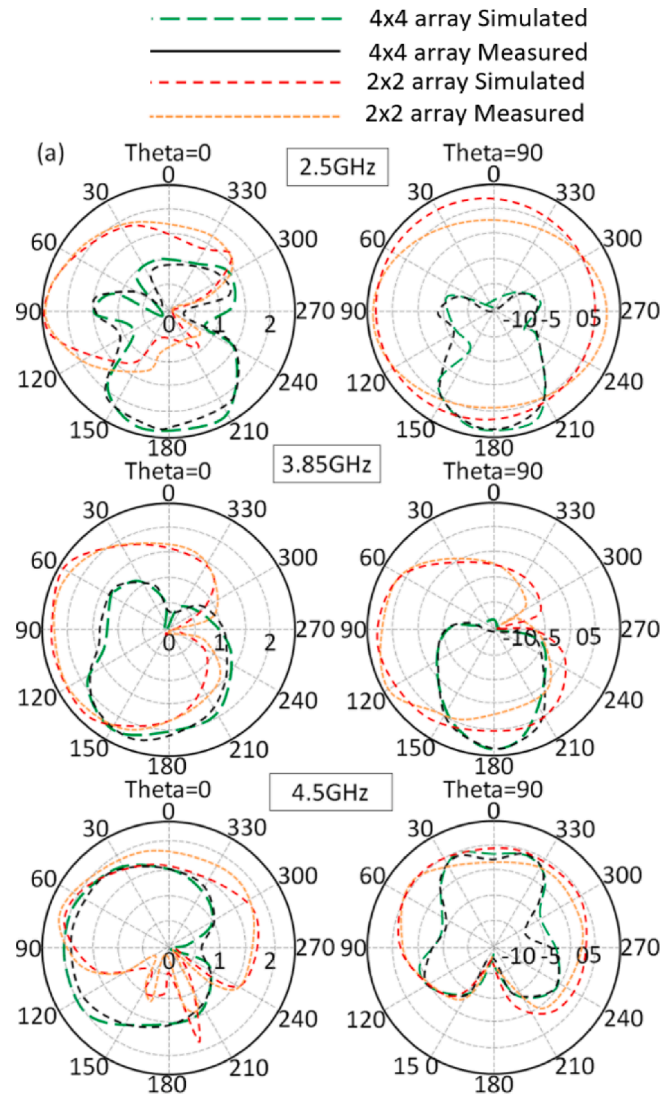
Fig. 19. Simulated and measured radiation patterns of the two-element and four-element antenna array at 2.5 GHz, 3.85 GHz, and 4.5 GHz.

backside of the antenna array are shown in Fig. 15. The two-element antenna arrays face each other to form a mirror image. The separation between the pair of antennas is 20 mm. All other dimensions remain the same as before as shown in Fig. 1. It should be noted that the CRLH filtering structure are conjoined as illustrated in Fig. 15, and the phase of the excitation signal at the four ports is identical. The reflection coefficient and isolation at all four ports of the 4 × 4 antenna array is shown in Fig. 16. It can be observed that the four-element array exhibits high isolation that is greater than 20 dB between adjacent radiating elements over its three bands. Also, the reflection coefficient across the triband is better than −18 dB at all ports. Compared to the responses of the 2 × 2 array in Fig. 11 with the CPW grounded, the 4 × 4 array has a better reflection coefficient response.

5. Experimental validation

The 2 × 2 and 4 × 4 antenna arrays were fabricated on standard FR4 substrate, which was specified earlier. The antenna array pattern was etched on the substrate using standard photolithography, also called optical lithography or UV lithography. This involves using light to transfer the geometric pattern of the array pattern from a photomask to a photosensitive chemical photoresist that had been applied on the

substrate. Chemical treatment was then applied to etch the UV exposed pattern into the substrate. The two fabricated prototype arrays are shown in Fig. 17.

The S-parameters and gain of the antenna arrays was measured using a Network Analyzer (Agilent PNA 8720). The measured results of the four-element reflection coefficient, the isolation between the ports and the antenna gain are shown in Fig. 18. The reflection coefficient is better than −10 dB across the three bands and the isolation between the ports is greater than 20 dB. Also, the array has a gain of ~ 5 dB across its bands. The results of the two-element array are very similar. The radiation patterns of the two-element and four-element antenna array were measured in an anechoic chamber. The radiation pattern at spot frequencies of at 2.5 GHz, 3.85 GHz, and 4.5 GHz are shown in Fig. 19. The results show very good agreement between the measured and simulated results.

Other important parameters characterizing the antenna array for MIMO applications are ECC, DG, Channel Capacity, and TRAC. Envelop correlation coefficient indicates the behavior of MIMO antennas. The simulated and measured ECC for the adjacent antennas in the 4 × 4 array is shown in Fig. 20 to be less than 0.08, which is acceptable for effective MIMO systems. The diversity gain indicates the loss that occurs in transmission power when the diversity scheme is performed using a
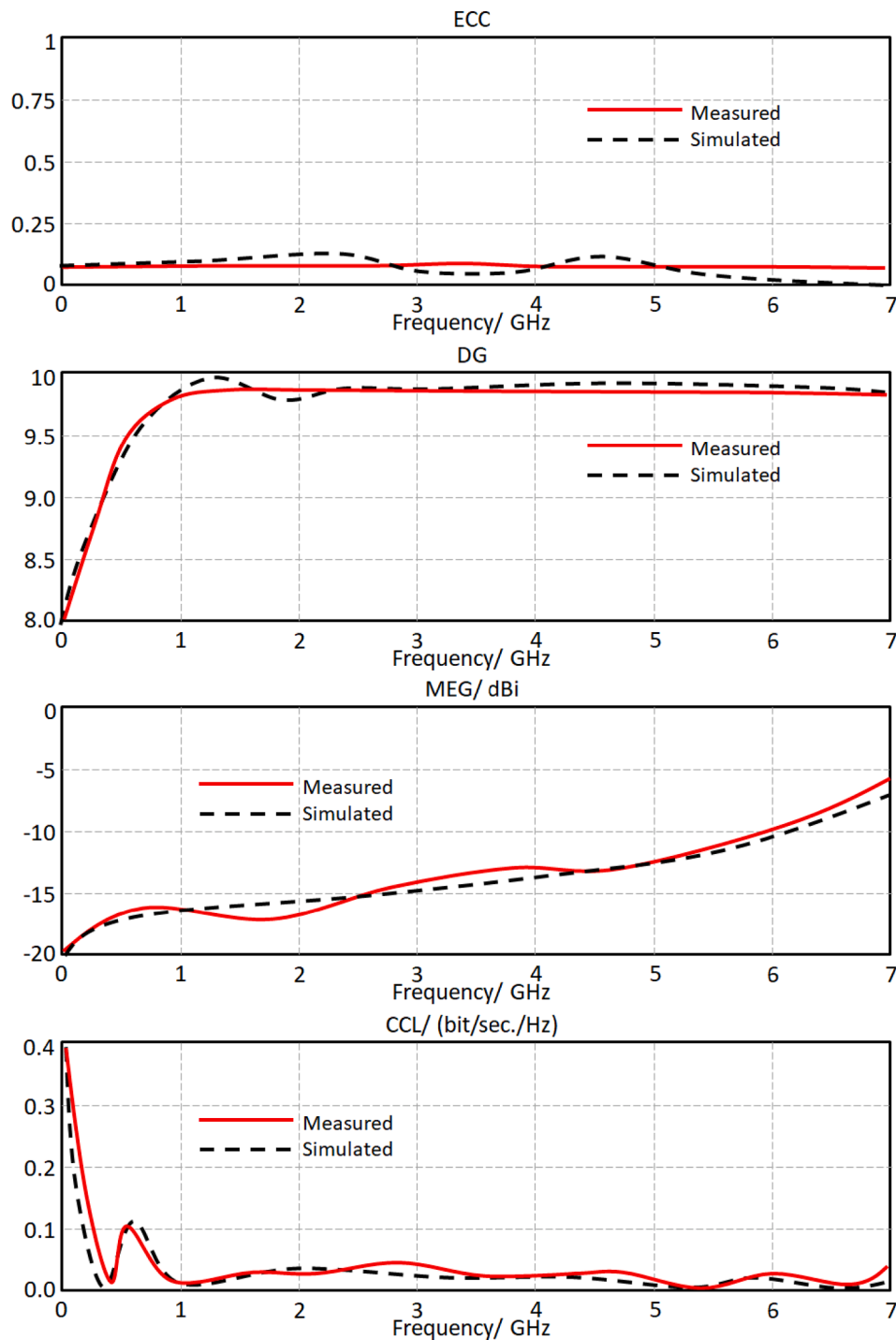
Fig. 20. Performance of the four-element antenna array in terms of envelope correlation coefficient (ECC), Diversity gain (DG), mean effective gain (MEG), and Channel capacity loss (CCL).

MIMO antenna array. Ideally, the DG should be 10 dB; however, in the case of the proposed 4 × 4 array it is 9.8 dB, which is acceptable for MIMO applications. The mean effective gain indicates the received power by a wireless system in a fading environment. The acceptable range of MEG should be < -6 dB, which is the case here. Channel capacity loss occurs in a communication system due to correlation effects. The formula provided in [25] can be utilized to estimate the CCL of a MIMO antenna array. Fig. 20 shows that measured value of CCL is < 0.05 (bits/s/Hz), which is acceptable for antenna arrays. Total Active Reflection Coefficient (TARC) is used to describe the coupling degree and channel independence between ports, in addition to the S-

parameters of individual ports. It can be calculated using the expression given in [26]. TARC between the antenna ports is less than −20 dB, which ensures low coupling effects and channel independence between receiver and transmitter in MIMO systems.

The proposed antenna is compared with antenna arrays recently reported in literature. Table 2 shows that compared to the other cited arrays is substantially smaller in size, offers higher gain, and the coupling between the ports is much smaller. It has comparable diversity gain (DG) as [32]. These features make it viable for MIMO applications in 5G wireless communications systems.

Table 2

Comparison of the proposed antenna array with recent works.

References	Antenna size (mm²)	Number of ports	Frequency bandwidth (GHz)	Maximum Gain (dBi)	Mutual coupling (dB)	DG (dB)	ECC	Gap between antennas
[26]	130 × 100	8	5.15–5.925	2.1	−15	—	0.05	λ/1.9
[27]	150 × 75	4	5.15–5.85	1.9	−14	9.8	0.06	λ/2
[28]	136 × 60	8	5.15–5.925	1.9	−10	9.3	0.09	λ/2
[29]	150 × 75	12	4.8–5.1	2.6	−12	9.7	—	λ/2.1
[30]	150 × 80	8	5.147–5.95	2.2	−10	9.2	0.11	λ/2.3
[31]	133 × 133	4	3.3–5.8	1.1	−15	9.3	0.10	λ/2.1
[32]	160 × 70	2	5.6–5.67	12	−30	10	0.06	λ/1.4
This work	30 × 40	4	2–3, 3.4–3.9, 4.4–5.2	6.3	−20	10	0.01	λ/15

6. Conclusion

We have demonstrated the design of a novel antenna array for sub-6 GHz 5G MIMO systems. The antennas in the array are based on Sierpiński triangle fractals that is backed with a composite right/left structure that effectively suppresses unwanted mutual coupling between the antennas. The antennas in the array are excited via an open-circuited feedline through a coplanar waveguide. The impedance bandwidth of the array is extended by embedding an inter-radiating element ground structure of low–high-low impedance. The low-impedance section is a staircase structure that closely follows the angled feedline to block near-field interaction between adjacent antennas. The performance of the antenna array was characterized practically to show it meets the MIMO systems requirements in terms of ECC, DG, channel capacity, and TRAC.

Declaration of Competing Interest

The authors declare that they have no known competing financial interests or personal relationships that could have appeared to influence the work reported in this paper.

Data availability

No data was used for the research described in the article.

References

[1] Desai A, Palandoken M, Byun JK, Nguyen TK. Wideband flexible/transparent connected-ground MIMO antennas for sub-6 GHz 5G and WLAN applications. IEEE Access 2021;9:147003–15.

[2] Ismail MM, Elwi TA, Salim AJ. A miniaturized printed circuit CRLH antenna-based Hilbert metamaterial array. J Commun Software Syst 2022;18(3):236–43.

[3] Al-Khaylani HH, Elwi TA, Ibrahim AA. Novel miniaturized reconfigurable microstrip antenna based printed metamaterial circuitries for 5G applications. Progr Electromagn Res C 2022;120:1–10.

[4] Neeta PK, Bahadure NB, Patil PD, Kulkarni JS. Flexible interconnected 4-port MIMO antenna for sub-6 GHz 5G and X band applications. AEU-Int J Electron C 2022;152:11–9.

[5] Kumar A, Mishra K, Mukherjee A, Chaudhary AK. Channel capacity enhancement using MIMO technology. In: Proc. IEEE Int. Conf. Adv. Eng., Sci. Manage. (ICAESM), Nagapattinam, India; 2012. p. 10–5.

[6] Zhang Z. Antenna Design for Mobile Devices, 2nd ed. Hoboken, NJ, USA: Wiley; 2017.

[7] Li Y, Sim C-Y-D, Luo Y, Yang G. 12-port 5G massive MIMO antenna array in sub-6 GHz mobile handset for LTE bands 42/43/46 applications. IEEE Access 2017;6:344–54.

[8] Hu W, et al. Dual-band ten-element MIMO array based on dual mode IFAs for 5G terminal applications. IEEE Access 2019;7:178476–85.

[9] Cui L, Guo J, Liu Y, Sim C-Y-D. An 8-element dual-band MIMO antenna with decoupling stub for 5G smartphone applications. IEEE Antennas Wireless Propag Lett Oct. 2019;18(10):2095–9.

[10] Zhao A, Ren Z. Size reduction of self-isolated MIMO antenna system for 5G mobile phone applications. IEEE Antennas Wireless Propag Lett Jan. 2019;18(1):152–6.

[11] Li Y, Sim C-Y-D, Luo Y, Yang G. High-isolation 3.5 GHz eight-antenna MIMO array using balanced open-slot antenna element for 5G smartphones. IEEE Trans Antennas Propag Jun. 2019;67(6):3820–30.

[12] Zhao X, Yeo SP, Ong LC. Decoupling of inverted-F antennas with high-order modes of ground plane for 5G mobile MIMO platform. IEEE Trans Antennas Propag Sep. 2018;66(9):4485–95.

[13] Chang L, Yu Y, Wei K, Wang H. Orthogonally polarized dual antenna pair with high isolation and balanced high performance for 5G MIMO smartphone. IEEE Trans Antennas Propag May 2020;68(5):3487–95.

[14] Chang L, Yu Y, Wei K, Wang H. Polarization-orthogonal co-frequency dual antenna pair suitable for 5G MIMO smartphone with metallic bezels. IEEE Trans Antennas Propag Aug. 2019;67(8):5212–20.

[15] Sun L, Li Y, Zhang Z, Feng Z. Wideband 5G MIMO antenna with integrated orthogonal-mode dual-antenna pairs for metal rimmed smartphones. IEEE Trans Antennas Propag Apr. 2020;68(4):2494–503.

[16] Ren Z, Zhao A, Wu S. MIMO antenna with compact decoupled antenna pairs for 5G mobile terminals. IEEE Antennas Wireless Propag Lett Jul. 2019;18(7):1367–71.

[17] Barani IRR, Wong K-L, Zhang Y-X, Li W-L. Low profile wideband conjoined open-slot antennas fed by grounded coplanar waveguides for 4×4 5G MIMO operation. IEEE Trans Antennas Propag Apr. 2020;68(4):2646–57.

[18] Sun L, Li Y, Zhang Z, Wang H. Self-decoupled MIMO antenna pair with shared radiator for 5G smartphones. IEEE Trans Antennas Propag May 2020;68(5):3423–32.

[19] Sun L, Li Y, Zhang Z. Decoupling between extremely closely spaced patch antennas by mode cancellation method. IEEE Trans Antennas Propag Jun. 2021;69(6):3074–83.

[20] Farahani HS, Veysi M, Kamyab M, Tadjalli A. Mutual coupling reduction in patch antenna arrays using a UC-EBG superstrate. IEEE Antennas Wireless Propag Lett 2010;9:57–9.

[21] Tang MC, et al. Mutual coupling reduction using meta-structures for wideband, dual-polarized, and high-density patch arrays. IEEE Trans Antennas Propag Aug. 2017;65(8):3986–98.

[22] Karmakar A. Fractal antennas and arrays: a review and recent developments. Int J Microw Wirel Technol 2020;13:173–97.

[23] Alnaiemy Y, Elwi TA, Nagy L. Mutual coupling reduction in patch antenna array based on EBG structure for MIMO applications. Periodica Polytechnica Electrical Engineering and Computer Science 2019;4:1–11.

[24] Guan Z, Zhao P, Lao Q, Wang X, Wang G. Parameter Extraction for Equivalent Circuit Model of RF Devices Based on a Hybrid Optimization Method. Electronics 2019;8:1–14.

[25] Zahra H, Awan WA, Ali WAE, Hussain N, Abbas SM, Mukhopadhyay S. A 28 GHz broadband helical inspired end-fire antenna and its MIMO configuration for 5G pattern diversity applications. Electronics 2021;10:405.

[26] Hen Z, Jin J. Compact quad-port MIMO antenna with ultra-wideband and high isolation. Electronics 2021;11(3408):1–22.

[27] Ren Z, Wu S, Zhao A. Triple band MIMO antenna system for 5G mobile terminals. In: Proceedings of the IEEE International Workshop on Antenna Technology (iWAT), 2019, pp. 163–165.

[28] Sim C, Liu H, Huang C. Wideband MIMO antenna array design for future mobile devices operating in the 5G NR frequency bands n77/n78/n79 and LTE band 46. IEEE Antennas Wirel Propag Lett 2020;19:74–8.

[29] Li Y, Sim CYD, Luo Y, Yang G. 12-Port 5G Massive MIMO antenna array in sub-6GHz mobile handset for LTE bands 42/43/46 applications. IEEE Access 2017;6:344–54.

[30] Guo J, Cui L, Li C, Sun B. Side-edge frame printed eight-port dual-band antenna array for 5G smartphone applications. IEEE Trans Antennas Propag 2018;66:7412–7.

[31] Abdulkawi WM, et al. Design of a compact dual-band MIMO antenna system with high-diversity gain performance in both frequency bands. Micromachines 2021;12(4):383.

[32] J.S.U. et al. A sub-6 GHz MIMO antenna array for 5G wireless terminals. Electronics, 2021, vol. 10, no. 24, pp. 12-18.

Sabah Hassan Ghadeer received the BSc. From University of Diylah, Department of Electrical Engineering collage of engineering, Iraq, 2005. He has a M.Sc. degree in Wireless Communication Centre from Universiti Teknologi Malaysia, Malaysia, 2091. His research interests are in the areas of wearable and implantable antennas, MIMO antenna array, self-powered wireless systems and smart antennas. Currently, he is perssuing his PhD in Faculty of Engineering, School of Electrical Engineering, Universiti Teknologi Malaysia (UTM) since 2020.

Sharul Kamal Abdul Rahim has been with the Wireless Communication Centre (WCC), a High Centre of Excellent (HICOE), UTM, Since 2001. Prior to his appointment with WCC, he was with the industry for 3 years. He was made Associate Professor at UTM in 2010 and Professor in 2017. His research interests include Antenna Design, Smart Antenna System and Beamforming Network for 5th Generation (5G) mobile communication. He holds an H-Index of 25 (SCOPUS) and more than 2000 citations (SCOPUS). He has authored various books and book chapters and published more than 250 technical papers in journals and proceedings including IEEE Trans. on Antenna and Propagation (TAP), IEEE Antennas and Wireless Propagation Letter (AWPL), IEEE Antenna Magazine, IEEE Access and Electronics Letters. He has served as a keynote and invited speaker at various International and session chair in many international conferences. He has received more than 56 academic and research awards. He has secured almost RM3M of research grant internationally and nationally as a head of projects. He has 10 patents granted and more that 30 patent filling and Copyright. On top of his academic achievement, he is a registered Professional Engineer since 2010. He is a member of the Senior Evaluation Panel for the Engineering Accreditation Council (EAC) of the Board of Engineers Malaysia (BEM). He was the Adjunct Professor at the University of Swinburne. He is also actively involved in The Institution of Engineers, Malaysia (Southern Branch) where he served as Vice Chairman (2016-2017) and Executive Committee (2012-2016). He is currently the Chairman of International Electrotechnical Commission of Technical Committee (TC 49) and (TC 124). He is also a Senior member of IEEE Malaysia Section, Member of Institution of Engineers Malaysia (MIEM), Member of the Institute of Electronics, Information and Communication Engineers (IEICE) and Eta Kappa Nu Chapter.

Mohammad Alibakhshikenari was born in Mazandaran, Iran, in February 1988. He received the Ph.D. degree (Hons.) with European Label in electronics engineering from the University of Rome "Tor Vergata", Italy, in February 2020. He was a Ph.D. Visiting Researcher at the Chalmers University of Technology, Sweden, in 2018. His training during the Ph.D. included a research stage in the Swedish company Gap Waves AB. He is currently with the Department of Signal Theory and Communications, Universidad Carlos III de Madrid (uc3m), Spain, as the Principal Investigator of the CONEX-Plus Talent Training Program and Marie Sklodowska-Curie Actions. He was also a Lecturer of the electromagnetic fields and electromagnetic laboratory with the Department of Signal Theory and Communications for academic year 2021–2022 and he received the "Teaching Excellent Acknowledgement" Certificate for the course of electromagnetic fields from Vice-Rector of studies of uc3m. His research interests include electromagnetic systems, antennas and wave-propagations, metamaterials and metasurfaces, synthetic aperture radars (SAR), multiple input multiple output (MIMO) systems, RFID tag antennas, substrate integrated waveguides (SIWs), impedance matching circuits, microwave components, millimeter-waves and terahertz integrated circuits, gap waveguide technology, beamforming matrix, and reconfigurable intelligent surfaces (RIS). He was a recipient of the three years research grant funded by Universidad Carlos III de Madrid and the European Union's Horizon 2020 Research and Innovation Program under the Marie Sklodowska-Curie Grant started in July 2021, the two years research grant funded by the University of Rome "Tor Vergata" started in November 2019, the three years Ph.D. Scholarship funded by the University of Rome "Tor Vergata" started in November 2016, and the two Young Engineer Awards of the 47th and 48th European Microwave Conference were held in Nuremberg, Germany, in 2017, and in Madrid, Spain, in 2018, respectively. His research article entitled "High-Gain Metasurface in Polyimide On-Chip Antenna Based on CRLH-TL for Sub Terahertz Integrated Circuits" published in Scientific Reports was awarded as the Best Month Paper at the University of Bradford, U.K., in April 2020. He is serving as an Associate Editor for (i) Radio Science, and (ii) IET Journal of Engineering. He also acts as a referee in several highly reputed journals and international conferences.

BAL S. VIRDEE graduated with a B.Sc. (Eng.) from the University of Leeds, U.K., and Ph.D. degree from the University of London, U.K. Since graduation he has worked in industry for various high-tech companies including Philips, as a research and development engineer, and at Teledyne Defence & Space as a future products developer in RF/microwave communications. He has taught in several academic institutions in the U.K. He is currently a senior professor of communications technology and director of center for communications technology at the school of computing and digital media, London Metropolitan University. He has supervised and examined numerous PhD students and has published extensively research papers at international conferences and peer-reviewed journals. His research, in collaboration with industry and academia, is in next generation wireless communications systems. He is Chair and Executive Member of the Institution of Engineering and Technology's (IET) technical and professional network committee on RF/microwave-technology. He is a charted engineer (CEng), Fellow of the IET and Senior Member of IEEE.

Taha A. Elwi received his B.Sc. in Electrical Engineering Department (2003) (Highest Graduation Award), Postgraduate M.Sc. in Laser and Optoelectronics Engineering Department (2005) (Highest Graduation Award) from Nahrain University Baghdad, Iraq. From April 2005 to August 2007, he was working with Huawei Technologies Company, Baghdad, Iraq. On January, 2008, he joined the University of Arkansas at Little Rock and he obtained his Ph.D. in December 2011 from the system engineering and science. His research areas include wearable and implantable antennas for biomedical wireless systems, smart antennas, WiFi deployment, electromagnetic wave scattering by complex objects, design, modeling and testing of metamaterial structures for microwave applications, design and analysis of microstrip antennas for mobile radio systems, precipitation effects on terrestrial and satellite frequency re-use communication systems, effects of the complex media on electromagnetic propagation and GPS. The nano-scale structures in the entire electromagnetic spectrum are a part of his research interest.

Amjad Iqbal received the B.S. degree in electrical engineering from COMSATS University, Islamabad, Pakistan, in 2016, the M.S. degree in electrical engineering from the CECOS University of IT and Emerging Science, Peshawar, Pakistan, in 2018, and the Ph.D. degree in engineering from Multimedia University, Cyberjaya, Malaysia, in 2021. He has worked as a Lab Engineer with the Department of Electrical Engineering, CECOS University, Peshawar, from 2016 to 2018. His research interests include printed antennas, flexible antennas, implantable antennas, multiple-input and multiple-output (MIMO) antennas, dielectric resonator antennas, wireless power transfer, and synthesis of microwave components.

Muath Al-Hasan received the B.A.Sc. degree in electrical engineering from the Jordan University of Science and Technology, Irbid, Jordan, in 2005, the M.A.Sc. degree in wireless communications from Yarmouk University, Irbid, in 2008, and the Ph.D. degree in telecommunication engineering from the Institut National de la Recherche Scientifique (INRS), Université du Québec, Montreal, QC, Canada, in 2015. From 2013 to 2014, he was with Planets Inc., San Francisco, CA, USA. In May 2015, he joined Concordia University, Montreal, Canada, as a Post-Doctoral Fellowship. He is currently an Assistant Professor with Al Ain University, Al Ain, United Arab Emirates. His current research interests include antenna design at millimeter-wave and terahertz, channel measurements in multiple-input and multiple-output (MIMO) systems, and machine learning and artificial intelligence in antenna design.